

2024-02-09

# Mitigating topological freezing using out-of-equilibrium simulations

Bonanno, C

<https://pearl.plymouth.ac.uk/handle/10026.1/22186>

---

10.48550/arxiv.2402.06561

---

*All content in PEARL is protected by copyright law. Author manuscripts are made available in accordance with publisher policies. Please cite only the published version using the details provided on the item record or document. In the absence of an open licence (e.g. Creative Commons), permissions for further reuse of content should be sought from the publisher or author.*

# Mitigating topological freezing using out-of-equilibrium simulations

---

**Claudio Bonanno,<sup>a</sup> Alessandro Nada,<sup>b</sup> Davide VDACCHINO<sup>c</sup>**

<sup>a</sup>*Instituto de Física Teórica UAM-CSIC, c/ Nicolás Cabrera 13-15, Universidad Autónoma de Madrid, Cantoblanco, E-28049 Madrid, Spain*

<sup>b</sup>*Dipartimento di Fisica, Università degli Studi di Torino and INFN, Sezione di Torino, Via Pietro Giuria 1, I-10125 Turin, Italy*

<sup>c</sup>*Centre for Mathematical Sciences, University of Plymouth, Plymouth, PL4 8AA, United Kingdom*  
*E-mail: [claudio.bonanno@csic.es](mailto:claudio.bonanno@csic.es), [alessandro.nada@unito.it](mailto:alessandro.nada@unito.it), [davide.vadacchino@plymouth.ac.uk](mailto:davide.vadacchino@plymouth.ac.uk)*

**ABSTRACT:** Motivated by the recently-established connection between Jarzynski's equality and the theoretical framework of Stochastic Normalizing Flows, we investigate a protocol relying on out-of-equilibrium lattice Monte Carlo simulations to mitigate the infamous computational problem of topological freezing. We test our proposal on  $2d$   $CP^{N-1}$  models and compare our results with those obtained adopting the Parallel Tempering on Boundary Conditions proposed by M. Hasenbusch, obtaining comparable performances. Our work thus sets the stage for future applications combining our Monte Carlo setup with machine learning techniques.

**KEYWORDS:** Algorithms and Theoretical Developments, Vacuum Structure and Confinement, Lattice Quantum Field Theory

---

## Contents

<b>1</b>	<b>Introduction</b>	<b>1</b>
<b>2</b>	<b>Numerical setup</b>	<b>3</b>
2.1	Lattice discretization of $2d$ $\text{CP}^{N-1}$ models	3
2.2	Out-of-equilibrium evolutions and Jarzynski's equality	6
<b>3</b>	<b>Numerical results</b>	<b>10</b>
3.1	Effective Sample Size and Kullback–Leibler divergence	10
3.2	Extracting the topological susceptibility	14
3.3	Integrated auto-correlation time of $\chi$	15
3.4	Efficiency of the method	16
<b>4</b>	<b>Conclusions</b>	<b>19</b>
<b>A</b>	<b>Evaluating <math>\hat{\text{ESS}}</math> as an estimator of the Effective Sample Size</b>	<b>20</b>
<b>B</b>	<b>Relation between the Effective Sample Size and the Kullback–Leibler divergence</b>	<b>20</b>

---

## 1 Introduction

It is well known that Markov Chain Monte Carlo simulations of lattice gauge theories based on local updating algorithms are affected by critical slowing down. The integrated auto-correlation time  $\tau$  associated with a given lattice observable  $\mathcal{O}$  diverges as the continuum limit is approached, in a way that is naturally described in terms of the correlation length  $\xi$  of the system.

While for lattice observables like the elementary plaquette or the Polyakov line  $\tau$  diverges as a power law,  $\tau \sim \xi^z$ , with  $z$  typically of order 2 or less, for topological quantities such as the topological charge  $Q$  this divergence is much more dramatic, see Refs. [1–18]. There is by now vast numerical evidence that both in  $4d$   $\text{SU}(N)$  gauge theories and in two-dimensional models, the divergence is exponential,  $\tau(Q) \sim e^\xi$ , see Refs. [5–7, 15].

Topological critical slowing down can be understood as follows. Sufficiently close to the continuum limit, a proper definition of topological charge is recovered for lattice gauge field configurations. This definition can be used to partition configuration space into sectors, separated by free energy barriers. The height of these barriers diverges with  $\xi$  and, as the continuum limit is approached, the disconnected topological sectors of the continuum theory emerge. The growth of the energy barriers also suppresses the tunneling rate of a Markov Chain generated by a local updating algorithm, that thus remains trapped in

one fixed topological sector. This effect, known as *topological freezing*, leads to a loss of ergodicity and introduces large systematic effects, especially in the calculation of topological observables such as the topological susceptibility.

Algorithms that exactly solve the problem of topological freezing are only known for specific low-dimensional toy models, see for example Ref. [14]. Yet, several suggestions have been made in the last few years to make the growth of  $\tau$  for topological observables milder, namely from exponential to polynomial. Examples are simulations with Open Boundary Conditions (OBCs) [9, 19], Parallel Tempering on Boundary Conditions (PTBC) [13, 16], metadynamics [10, 20], density of states methods [21, 22], master field simulations [23], machine-learning based approaches such as Normalizing Flows [24–27], and many others [28–31].

In this study, we propose a novel algorithm aimed at mitigating topological freezing. As our strategy builds on features of simulations with OBCs as well as on the PTBC algorithm proposed by M. Hasenbusch in Ref. [13], we briefly summarize their main properties below.

In theories defined on a continuum space-time, topological charge is integer valued as a consequence of Periodic Boundary Conditions (PBCs) in time. Abandoning PBCs in favour of OBCs corresponds to eliminating the barriers between topological sectors, which are not disconnected anymore. Performing Monte Carlo simulations with OBCs thus allows the Markov Chain to switch topological sector more easily, resulting in a dramatic reduction of topological auto-correlation time. In particular, it was shown in Ref. [9, 19] that the divergence of  $\tau$  is reduced to a polynomial one,  $\tau \sim \xi^2$ . Yet, this approach suffers from some drawbacks. As a matter of fact, OBCs introduce nonphysical effects, which have to be avoided by only computing correlation functions in the bulk of the lattice. Hence, larger volumes are required in order to keep finite size effects under control while still avoiding unwanted systematic errors. In this respect, the PTBC algorithm, proposed for  $2d$   $CP^{N-1}$  models in Ref. [13] and recently implemented also for  $4d$   $SU(N)$  gauge theories in Ref. [16] aims at having the best of both worlds. By combining PBCs and OBCs simulations in the framework of the parallel tempering idea, it exploits the improved scaling of the auto-correlation time of the topological charge in systems with OBCs simulations while, at the same time, avoiding the drawbacks mentioned above, as physical quantities are computed with PBCs. The PTBC algorithm has been recently employed in a variety of cases, demonstrating a dramatic reduction of the auto-correlation time of the topological charge, and improving state-of-the-art results for several topological and non-topological quantities [16, 32–37].

The strategy proposed in this study shares its roots with the PTBC algorithm, as it still combines the use of Open and Periodic boundary conditions. However, it makes use of *out-of-equilibrium evolutions* based on the well-known Jarzynski’s equality, see Ref. [38]. A fundamental result of non-equilibrium statistical mechanics, Jarzynski’s equality has been extensively used in recent years in several contexts in lattice field theories, ranging from the computation of interface free energies, see Ref. [39], of the QCD equation of state, see Ref. [40], of renormalized coupling of  $SU(N)$  gauge theories, see Ref. [41], and in the study of the entanglement entropy from the lattice, see Ref. [42].

The underlying idea is to sample the configuration space of the system with PBCs using

a previous sampling of the configuration space of the system with OBCs, the latter being used as a starting point for non-equilibrium evolutions. Using Jarzynski’s equality, the expectation values of the desired observables can then be obtained for the system with PBCs through a reweighting procedure. In this approach, the decorrelation of the topological charge still benefits from the presence of OBCs, while avoiding their pitfalls, with a cost overhead that will be quantified by the length of the out-of-equilibrium trajectory.

The main motivation behind the present study is a recent development in the field of machine-learning based on the combination of Jarzynski’s equality with Normalizing Flows (NFs). In this new framework, known as Stochastic Normalizing Flows (SNFs), see Refs. [43, 44], out-of-equilibrium Monte Carlo evolutions are combined with discrete coupling layers (the same building blocks composing NFs) to achieve a substantial improvement of sampling efficiency with respect to a purely stochastic approach. As our strategy is rooted on Jarzynski’s equality too, SNFs would be a natural future direction for the application of our proposal.

The aim of the present study is thus to probe the use of the out-of-equilibrium methods in the computation of the topological observables in order to set the stage for this future development. Its technical feasibility will be explored, and its performance compared with that of the PTBC algorithm. We will focus on the  $2d$   $CP^{N-1}$  models, see Refs. [45–48], which are a very popular test bed for new numerical approaches, see Refs. [6, 13, 15, 32, 49–55]. They are generally simpler to study on the lattice compared to QCD while still exhibiting non-trivial topological features, which they share with  $4d$   $SU(N)$  gauge theories. A preliminary version of the results discussed in this manuscript was presented at the 2023 Lattice Conference, and can be found in Ref. [56].

This paper is organized as follows. In Section 2 we introduce the numerical setup used in this study, with a heavy focus on the features of out-of-equilibrium evolutions. The numerical results obtained with this method are presented and discussed in Section 3. Finally, in Section 4 we draw our conclusions and point to the future directions of this investigation.

## 2 Numerical setup

In this section, the numerical setup used in this study is introduced. The  $2d$   $CP^{N-1}$  models are defined, along with the local updating algorithm used to generate their configurations. Out-of-equilibrium methods are also introduced, along with a detailed explanation on how they are used to carry out the program sketched above.

### 2.1 Lattice discretization of $2d$ $CP^{N-1}$ models

Consider the following continuum Euclidean action of  $2d$   $CP^{N-1}$  models [45, 46]:

$$S[\bar{z}, z, A] = \int d^2x \left[ \frac{N}{g} \bar{D}_\mu \bar{z}(x) D_\mu z(x) \right], \quad (2.1)$$

where  $g$  is the ’t Hooft coupling,  $z = (z_1, \dots, z_N)$  is a  $N$ -component complex scalar satisfying  $\bar{z}z = 1$ , and  $D_\mu \equiv \partial_\mu + iA_\mu$  is the  $U(1)$  covariant derivative, where  $A_\mu(x)$  is a

non-propagating U(1) gauge field<sup>1</sup>. An integer-valued topological charge can be conveniently expressed in terms of the gauge field according to Refs. [45, 46] as follows,

$$Q = \frac{1}{2\pi} \epsilon_{\mu\nu} \int d^2x \partial_\mu A_\nu(x) \in \mathbb{Z}, \quad (2.2)$$

while the topological susceptibility, which is our main observable of interest, is defined as usual as (here  $V$  is the space-time volume):

$$\chi = \lim_{V \rightarrow \infty} \frac{\langle Q^2 \rangle}{V}. \quad (2.3)$$

We discretize the action, Eq. (2.1), on a square lattice of size  $L$ , using the  $O(a)$  tree-level Symanzik-improved lattice action defined in Ref. [50]. A crucial ingredient in this study is the choice of boundary conditions. They are imposed as periodic in every direction and for every point of the boundary of the lattice, except for a segment of length  $L_d$  along the spatial boundary. In the following, this segment will be known as *defect* and will be denoted by  $D$ . Along the defect we impose OBCs. Our purpose is to gradually evolve these to PBCs using the out-of-equilibrium evolutions described in Sec. 2.2. This choice of boundary conditions can be encoded directly into the dynamics by considering the following family of lattice actions, each labeled by an integer  $n$ ,

$$S_L^{(n)}[\bar{z}, z, U] = -2N\beta \sum_{x,\mu} \left\{ k_\mu^{(n)}(x) c_1 \Re [\bar{U}_\mu(x) \bar{z}(x + \hat{\mu}) z(x)] + k_\mu^{(n)}(x + \hat{\mu}) k_\mu^{(r)}(x) c_2 \Re [\bar{U}_\mu(x + \hat{\mu}) \bar{U}_\mu(x) \bar{z}(x + 2\hat{\mu}) z(x)] \right\}, \quad (2.4)$$

where  $\beta$  is the inverse bare 't Hooft coupling,  $c_1 = 4/3$  and  $c_2 = -1/12$  are Symanzik-improvement coefficients, and  $U_\mu(x) = \exp\{i\phi_\mu(x)\}$  are the U(1) gauge link variables. The factors  $k_\mu^{(n)}(x)$  appearing in Eq. (2.4) are used to implement different boundary conditions for the link variables crossing the defect  $D$ . They are defined as follows,

$$k_\mu^{(n)}(x) \equiv \begin{cases} c(n), & x \in D \wedge \mu = 0, \\ 1, & \text{otherwise,} \end{cases} \quad (2.5)$$

with  $0 \leq c(n) \leq 1$  a function that interpolates between  $c = 0$  and  $c = 1$  corresponding, respectively, to OBCs and PBCs. The setup described above is sketched in Fig. 1.

The behaviour of the model defined above can be clarified as follows. When  $c = 1$ , the factors  $k_\mu^{(n)}(x)$  are everywhere equal to 1. Then, the action in Eq. (2.4) reduces to the standard Symanzik-improved action of  $2d$   $\text{CP}^{N-1}$  models with PBCs. When  $0 \leq c < 1$ , the coupling  $\beta$  on the links crossing  $D$  get suppressed by a factor of  $c$  each. This corresponds to a suppression of the force entering the updating procedure for those specific links and of the corresponding site variables, and to its vanishing when  $c = 0$ . In the latter case, the site and link variables involved will not be updated at all and will thus remain unchanged

---

<sup>1</sup>The non-propagating gauge field  $A_\mu(x)$  could be integrated out and expressed in terms of  $z(x)$  [46, 47]. However, this formulation is more convenient for the purpose of lattice simulations.

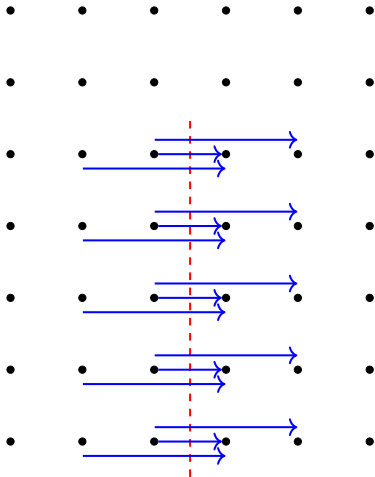


**Figure 1:** Figure taken from Ref. [32]. The dashed line represents the defect  $D$ , while the solid arrows represent links or product of links crossing the defect orthogonally, and thus getting suppressed by factor(s) of  $c(n)$  according to the definition of  $k_{\mu}^{(n)}(x)$  in Eq. (2.5). In this case the defect is placed on the space boundary (i.e., along the  $\mu = 1$  direction), so that only temporal links  $U_0$  will cross it.

during the Monte Carlo evolution, thus realizing OBCs. In this work we chose a simple linear interpolation between OBCs and PBCs, namely,  $c(n) = n/n_{\text{step}}$ , with  $c(n = 0) = 0$  (OBCs case) and  $c(n_{\text{step}}) = 1$  (PBCs case).

For the updating procedure, we relied on the standard 4:1 combination of Over-Relaxation (OR) and over-Heat-Bath (HB) local update algorithms, see Ref. [50] for more details. The full lattice update sweeps were supplemented with *hierarchical* updates of subregions of the lattice centered on the defect. These allow to update the links and sites close to  $D$ , where the creation/annihilation of new topological excitations occurs most likely, thereby improving the evolution of the Markov Chain between topological sectors. These hierarchical updates were designed along the same lines of Ref. [13], where more details may be found. Hierarchical updates were alternated with translations in randomly-chosen directions by one lattice spacing of the position of the defect on the periodic replica (which is translation-invariant), so that topological excitations are created/annihilated in different places around the lattice. Such translations are effectively achieved by simply translating the site/link variables of the periodic field configurations.

As discussed in the Introduction, the measurement of lattice out-of-equilibrium evolutions happens on systems with PBCs. In the case of PBCs, no unphysical effects coming from the fixed boundaries are present and we can safely rely on several different discretizations of the global topological charge defined in Eq. (2.2) for the  $2d$   $\text{CP}^{N-1}$  models on a torus. In this study, we will adopt the so called *geometric* definition as in Ref. [50], which is known to be integer valued for every lattice configuration,

$$Q_{\text{geo}}[U] = \frac{1}{2\pi} \sum_x \Im \{ \log [\Pi_{01}(x)] \} \in \mathbb{Z}, \quad (2.6)$$

where  $\Pi_{\mu\nu}(x) \equiv U_{\mu}(x)U_{\nu}(x + a\hat{\mu})\bar{U}_{\mu}(x + a\hat{\nu})\bar{U}_{\nu}(x)$  is the elementary plaquette.

The geometric lattice topological charge in Eq. (2.6) is computed on configurations that have undergone a small amount of smoothing of the gauge and matter fields. This is done in order to remove the effects of ultraviolet (UV) fluctuations at the scale of the lattice spacing. Several different smoothing methods have been proposed in the literature, such as cooling, see Refs. [57–63], stout smearing, see Refs. [64, 65] or gradient flow, see Refs. [66, 67]. From the numerical standpoint, all these methods have been shown to give consistent results when properly matched to one another, see Refs. [63, 68, 69]. In this study, we adopt cooling for its simplicity and for its limited numerical cost. A single cooling step consists in aligning, site by site and link by link, each variable  $z(x)$  and  $U_\mu(x)$  to their corresponding local forces. As shown in Ref. [69], the specific action from which the local force is computed does not need to be the one used for the Monte Carlo evolution. Thus, we rely on the non-improved action, i.e., the action in Eq. (2.4) with  $c_1 = 1$  and  $c_2 = 0$ . The topological charge was evaluated using the geometric definition after a fixed number of 20 cooling steps, as its value was systematically observed to stabilize after 10 steps. In the end, the topological susceptibility will then be defined on a finite lattice as follows,

$$a^2\chi = \frac{\langle Q^2 \rangle}{L^2}, \quad (2.7)$$

where  $Q \equiv Q_{\text{geo}}^{(\text{cool})} \in \mathbb{Z}$  is the integer-valued lattice geometric topological charge computed after cooling, and where the meaning of the mean over the ensemble in our out-of-equilibrium setup will be clarified in the next section.

## 2.2 Out-of-equilibrium evolutions and Jarzynski’s equality

In this subsection, we explain in detail how Jarzynski’s equality enables us to compute vacuum expectation values in the system with PBCs (the *target* distribution), starting from a sampling of the system with OBCs (the *prior* distribution).

Consider the following family of partition functions,

$$\mathcal{Z}_{c(n)} \equiv \int [d\bar{z}dzdU] e^{-S_L^{(n)}[\bar{z},z,U]}. \quad (2.8)$$

Each one corresponds to a system described by action in Eq. (2.4) with boundary conditions specified by the parameter  $c$ . The prior system with OBCs will then correspond to  $c(n=0) = 0$ , with partition function  $\mathcal{Z}_0$ , while the target system with PBCs will instead correspond to  $c(n=n_{\text{step}}) = 1$ , with partition function  $\mathcal{Z}_1 \equiv \mathcal{Z}$ .

A sampling of the target distribution is obtained from a sampling of the prior distribution through out-of-equilibrium evolutions. Along the evolution, the boundary condition parameter is gradually changed from  $c = 0$  to  $c = 1$ . The change is effected in  $n_{\text{step}}$  steps. At each step  $n$ , the change from  $c(n)$  to  $c(n+1)$  is followed by a number of configuration updates<sup>2</sup>. These combined operations allow us to define a transition probability distribution  $\mathcal{P}_n(\phi_{n-1} \rightarrow \phi_n)$  where  $\phi_{n-1}$  and  $\phi_n$  collectively denote the elementary degrees of freedom  $z$  and  $U$  at step  $n-1$  and  $n$ , respectively. As just a few updates are performed after every

---

<sup>2</sup>The update algorithm must satisfy detailed balance.



change in  $c$ , the system with elementary degrees of freedom  $\phi_n$  can be considered to be out of equilibrium.

Jarzynski's equality allows to compute the ratio between the partition functions of the target and prior distributions,

$$\frac{\mathcal{Z}}{\mathcal{Z}_0} = \langle \exp\{-W\} \rangle_f, \quad (2.9)$$

where

$$W[\phi_0, \dots, \phi_{n_{\text{step}}-1}] \equiv \sum_{n=0}^{n_{\text{step}}-1} \left\{ S_L^{(n+1)}[\phi_n] - S_L^{(n)}[\phi_n] \right\} \quad (2.10)$$

is known as *generalized work*. The out-of-equilibrium average  $\langle \mathcal{A} \rangle_f$  is defined as follows,

$$\langle \mathcal{A} \rangle_f = \int [d\phi_0 \dots d\phi] q_0[\phi_0] \mathcal{P}_f[\phi_0, \dots, \phi] \mathcal{A}[\phi_0, \dots, \phi], \quad (2.11)$$

where  $\phi \equiv \phi_{n_{\text{step}}}$  denotes the configuration reached at the end of the out-of-equilibrium evolution. In the above,  $\mathcal{P}_f[\phi_0, \dots, \phi] \equiv \prod_{n=1}^{n_{\text{step}}} \mathcal{P}_n(\phi_{n-1} \rightarrow \phi_n)$  is the total transition probability of the out-of-equilibrium evolution, and  $q_0[\phi_0] \equiv \mathcal{Z}_0^{-1} \exp\{-S_L^{(0)}[\phi_0]\}$  the probability of drawing the field configuration  $\phi_0$  from the prior distribution.

Using Eq. (2.9) and Eq. (2.11), one can show that the expectation value of an observable  $\mathcal{O}$  with respect to the target distribution can be expressed as follows,

$$\langle \mathcal{O} \rangle_{\text{NE}} = \frac{\langle \mathcal{O}[\phi] \exp\{-W[\phi_0, \dots, \phi_{n_{\text{step}}-1}]\} \rangle_f}{\langle \exp\{-W[\phi_0, \dots, \phi_{n_{\text{step}}-1}]\} \rangle_f} \quad (2.12)$$

where the NE denotes the fact that a Non-Equilibrium method has been used for the computation.

In the following, our strategy will thus be to start from an ensemble of configurations  $\{\phi_0\}$ , sampled from the prior distribution  $q_0$ , i.e., using action Eq. (2.4) with  $c(0) = 0$ , and to perform, for each configuration, the out-of-equilibrium evolution defined above. Of course, there is no unique way to interpolate from  $c = 0$  to  $c = 1$ . Hence, we supplement the above procedure with a *protocol*,

$$\phi_0 \xrightarrow{c(0) \rightarrow c(1)} \phi_1 \xrightarrow{c(1) \rightarrow c(2)} \phi_2 \quad \dots \quad \phi_{n_{\text{step}}-1} \xrightarrow{c(n_{\text{step}}-1) \rightarrow c(n_{\text{step}})} \phi_{n_{\text{step}}} \equiv \phi, \quad (2.13)$$

that is, with a choice for the value of  $c(n)$  for each step.

While it is necessary to perform a measurement of the action at each step in order to obtain the generalized work from Eq. (2.10), the measurement of the observable of interest  $\mathcal{O}$  is only performed at the end of the out-of-equilibrium evolution. In other words, the observable is only measured when the system has reached PBCs, thus avoiding unphysical effects introduced by OBCs. A sketch of our overall algorithmic procedure is displayed in Fig. 2.

As is also evident from Eq. (2.12), the technique laid out above has conceptual similarities with common reweighting techniques. It is natural to expect the *quality* of sampling

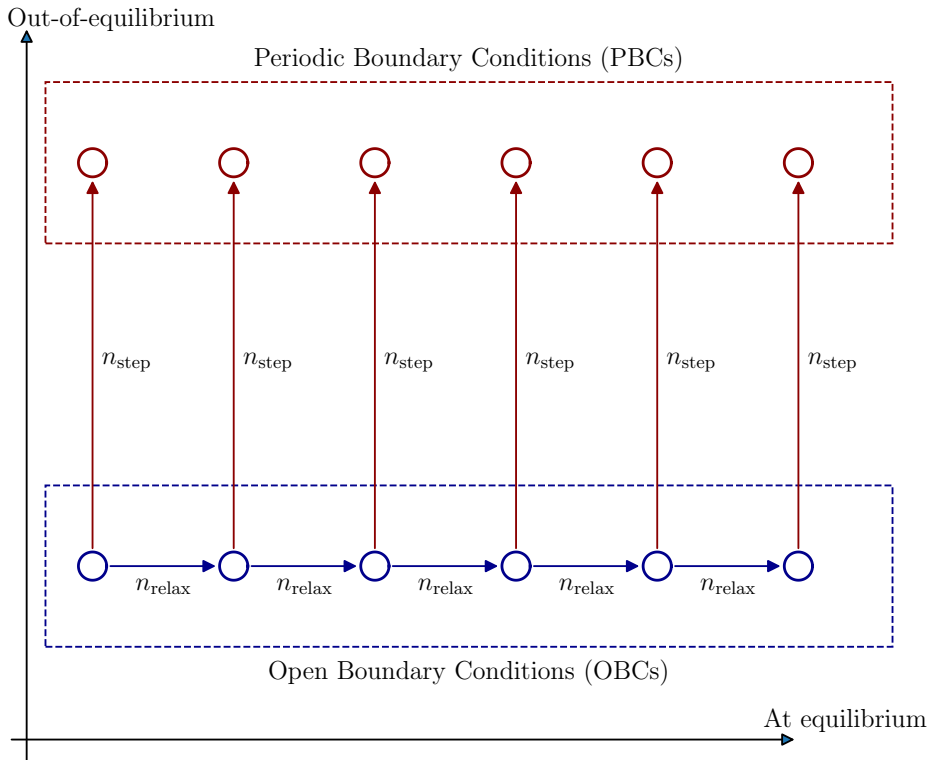


**Figure 2:** Sketch of the out-of-equilibrium setup. The horizontal axis represents the Monte Carlo time, where a new configuration is generated at equilibrium every  $n_{\text{relax}}$  updating steps according to the prior distribution, i.e., with OBCs. The vertical arrows instead stand for the  $n_{\text{ev}}$  out-of-equilibrium evolutions used to gradually switch on PBCs, each of these  $n_{\text{step}}$  steps long. The bullets correspond to the states of the system. Observables are computed only at the end of the out-of-equilibrium evolution, while the work is computed all along.

of the target distribution to depend on the overlap between the successive distributions in  $\mathcal{Z}_c$ , which is expected to be smaller for evolutions that are farther from equilibrium. Since too far out-of-equilibrium evolutions could lead to a small signal-to-noise ratio and/or to a possibly large bias in the computation of  $\langle \mathcal{O} \rangle_{\text{NE}}$  through Eq. (2.12), it is important to quantify the distance of the chosen evolution from equilibrium.

A figure of merit designed to fit that purpose is the reverse Kullback–Leibler divergence  $\tilde{D}_{\text{KL}}$ , which is a measure of the similarity between two probability distributions and it is defined to be always larger or equal to zero. In general, the simplest choice would be to compute the overlap between the target distribution and the one that has been generated at the end of an out-of-equilibrium evolution. The corresponding Kullback–Leibler divergence is:

$$\tilde{D}_{\text{KL}}(q||p) = \int d\phi q(\phi) \log \left( \frac{q(\phi)}{p(\phi)} \right), \quad (2.14)$$

where  $p \equiv \mathcal{Z}^{-1} \exp\{S_L^{(n_{\text{step}})}\}$  is the probability of drawing a configuration from the target

distribution, while  $q$  is a (generally intractable) distribution of the form

$$q(\phi) = \int [d\phi_0 \dots d\phi_{n_{\text{step}}-1}] q_0[\phi_0] \mathcal{P}_f[\phi_0, \dots, \phi]. \quad (2.15)$$

For out-of-equilibrium evolutions we have no direct access to  $q$  and this prevents us from computing the quantity in Eq. (2.14). However, another, different, Kullback–Leibler divergence can be defined by comparing the forward and reverse transition probabilities between  $\phi_0$  and  $\phi$ . Labeling the former by f, see Eq. (2.13), and the latter by r, we have:

$$\tilde{D}_{\text{KL}}(q_0 \mathcal{P}_f \| p \mathcal{P}_r) = \int [d\phi_0 \dots d\phi] q_0[\phi_0] \mathcal{P}_f[\phi_0, \dots, \phi] \log \left( \frac{q_0[\phi_0] \mathcal{P}_f[\phi_0, \dots, \phi]}{p[\phi] \mathcal{P}_r[\phi, \dots, \phi_0]} \right). \quad (2.16)$$

This quantity is directly related to thermodynamic quantities: if  $\Delta F \equiv -\log \frac{\mathcal{Z}}{\mathcal{Z}_0}$  is the variation of the free energy along the out-of-equilibrium evolution and  $W$  the corresponding (generalized) work from Eq. (2.10), then it is easy to derive (using detailed balance) that

$$\tilde{D}_{\text{KL}}(q_0 \mathcal{P}_f \| p \mathcal{P}_r) = \langle W \rangle_f + \log \frac{\mathcal{Z}}{\mathcal{Z}_0} = \langle W \rangle_f - \Delta F \geq 0. \quad (2.17)$$

For an equilibrium process, for which  $\tilde{D}_{\text{KL}} = 0$ , we have that  $\langle W \rangle_f = \Delta F$ , i.e., all of the work spent in the out-of-equilibrium evolution is transferred into the free energy difference between the prior and the target distributions; this is exactly the expectation for a reversible evolution through equilibrium states, for which there is no difference between forward and reverse. For a generic out-of-equilibrium process we have instead  $\tilde{D}_{\text{KL}} > 0$ , that corresponds to evolutions for which the probabilities of the forward and reverse evolutions are different. From a thermodynamic perspective this implies, instead,  $\langle W \rangle_f > \Delta F$ , i.e., part of the work is dissipated. It is then clear that Eq. (2.17) is a restatement of the Second Principle of Thermodynamics. Finally, it is easy to prove that:

$$\tilde{D}_{\text{KL}}(q \| p) \leq \tilde{D}_{\text{KL}}(q_0 \mathcal{P}_f \| p \mathcal{P}_r). \quad (2.18)$$

Thus, the value of the divergence of Eq. (2.16) also puts a constraint on how far the actual generated distribution  $q$  is from the target distribution  $p$ .

Another figure of merit that can be used to quantify the distance from equilibrium is the so-called *Effective Sample Size* (ESS). This quantity is customarily employed in the context of (Stochastic) Normalizing Flows as it encapsulates the relationship between the variance of an observable sampled directly from the target distribution  $p$  and the variance of the same observable obtained using Eq. (2.12). Ignoring auto-correlations, it is easy to show that

$$\frac{\text{Var}(\mathcal{O})_{\text{NE}}}{n} = \frac{\text{Var}(\mathcal{O})_p}{n \text{ESS}}, \quad (2.19)$$

which also motivates the name *Effective Sample Size*. The variance of an observable  $\mathcal{O}$ , obtained through Eq. (2.12), is equal to the variance obtained from the target distribution  $p$  with a smaller sample of size  $n_{\text{eff}} = \text{ESS} \times n \leq n$ .

In this study, we employ the following estimator:

$$\text{E}\hat{\text{SS}} \equiv \frac{\langle e^{-W} \rangle_f^2}{\langle e^{-2W} \rangle_f} = \frac{1}{\langle e^{-2(W-\Delta F)} \rangle_f}, \quad (2.20)$$

and we refer to Ref. [70] for a discussion on how  $\text{E}\hat{\text{SS}}$  is related to the true Effective Sample Size of Eq. (2.19). The estimator  $\text{E}\hat{\text{SS}}$  can be easily related to the variance of the weights  $e^{-W}$  appearing in Eq. (2.12). Indeed, since  $\text{Var}(e^{-W}) = \langle e^{-2W} \rangle_f - \langle e^{-W} \rangle_f^2 \geq 0$ , then

$$\text{Var}(e^{-W}) = \left( \frac{1}{\text{E}\hat{\text{SS}}} - 1 \right) \langle e^{-W} \rangle_f^2 = \left( \frac{1}{\text{E}\hat{\text{SS}}} - 1 \right) e^{-2\Delta F} \geq 0, \quad (2.21)$$

and, as a consequence,

$$0 < \text{E}\hat{\text{SS}} \leq 1. \quad (2.22)$$

From the above we see that  $\text{E}\hat{\text{SS}} = 1$  implies  $\text{Var}(e^{-W}) = 0$ , which is only possible if the weights  $e^{-W}$  are all equal. In this case, it is apparent from Eq. (2.12) that no reweighting is being done at all, and we are at equilibrium. On the other hand, a value of  $\text{E}\hat{\text{SS}}$  approaching zero signals sizeable fluctuations in the weights  $e^{-W}$ , corresponding to a noisy reweighting and to out-of-equilibrium evolutions.

### 3 Numerical results

This section is devoted to the discussion of the numerical results concerning the efficiency of the use of out-of-equilibrium evolutions, which will be measured in terms of the auto-correlation time of  $\chi$ .

In Ref. [13], the PTBC algorithm was shown to outperform standard local algorithms both in the presence of PBCs and OBCs. Moreover, it was shown to enjoy smaller auto-correlation times with respect to other setups, such as metadynamics simulations, see Ref. [10]. Hence, in the following, a direct comparison between the performance of the out-of-equilibrium protocol and of parallel tempering will be performed.

Since our goal is to test the robustness of the method, we have chosen to probe a wide array of different combinations of  $L_d$ ,  $n_{\text{step}}$  and  $n_{\text{relax}}$  in independent simulations, rather than obtaining larger samples for a smaller number of setups.

Thus, simulations for two different values of the parameter  $N$  specifying the model were performed, and we focused, for each value of these, on a single value of  $\beta$  and  $L$ , see Tab. 1. These simulation setups were chosen to enable direct comparison with previous results from Refs. [32, 33]. However, for a few choices of  $L_d$  and  $n_{\text{step}}$  we will also present results for the auto-correlation time obtained with our out-of-equilibrium setup varying the lattice spacing and/or the volume.

#### 3.1 Effective Sample Size and Kullback–Leibler divergence

As a first step in the investigation of the performance of our new proposal, we study how both the Kullback–Leibler divergence  $\tilde{D}_{\text{KL}}$  and the Effective Sample Size  $\text{E}\hat{\text{SS}}$  depend on  $n_{\text{step}}$  and on the defect length  $L_d$ .

$N$	$\beta$	$L$	$L_d$	$n_{\text{step}}$	$n_{\text{relax}}$
21	0.7	114	[6,114]	[200,2000]	[50,250]
41	0.65	132	[10,30]	[500,2000]	[50,250]

**Table 1:** Setup of the numerical simulations. The model is specified by  $N$ ,  $\beta$  and the size of the square lattice  $L$ . Non-equilibrium evolutions are characterized by the choice of the length  $L_d$  of the line defect, the length of the evolution  $n_{\text{step}}$  and the intermediate number of updating steps between each out-of-equilibrium evolution  $n_{\text{relax}}$ .

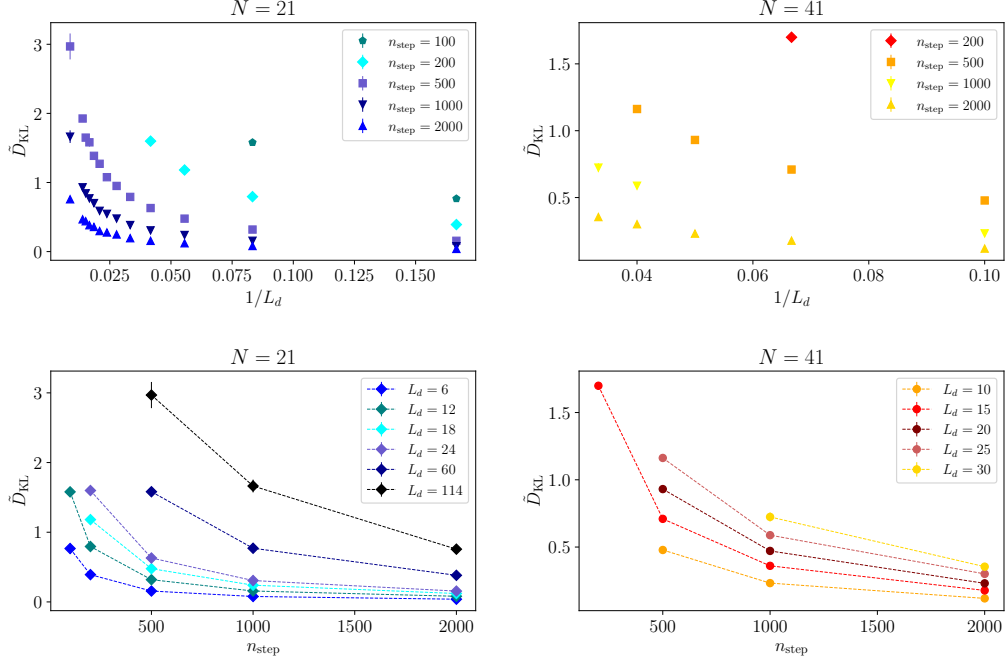


**Figure 3:** Behavior of the  $\tilde{D}_{\text{KL}}$  as a function of  $n_{\text{step}}$  (lower panels) and of the inverse of the defect size  $L_d$  (upper panels), for  $N = 21$  (left panels) and  $N = 41$  (right panels).

The aim of this section is, in particular, to quantify the distance of Jarzynski evolutions from equilibrium as the parameters  $n_{\text{step}}$  and  $L_d$  are varied. This is a crucial step in order to assess the reliability of the exponential Jarzynski reweighting.

On general grounds, we expect the Kullback–Leibler divergence to approach zero, its expected value at equilibrium, when either  $n_{\text{step}}$  is increased at fixed  $L_d$  or  $L_d$  is increased at fixed  $n_{\text{step}}$ . The expectation explain above is clearly confirmed in Fig. 3, where  $\tilde{D}_{\text{KL}}$  is displayed as a function of  $1/L_d$  and  $n_{\text{step}}$  for fixed  $n_{\text{relax}}$ .

The behaviour of E $\hat{\text{S}}$ S reflects the same picture. The evolution towards the target distribution is expected to approach equilibrium as  $n_{\text{step}}$  is increased and to recede from it as  $L_d$  is increased at fixed  $n_{\text{step}}$ . Accordingly, E $\hat{\text{S}}$ S is expected to approach 1 in the former case, and to recede from it in the latter. This is indeed what can be observed in Fig. 4, where E $\hat{\text{S}}$ S is displayed as a function of  $1/L_d$  and of  $n_{\text{step}}$ , in the left and right panels, respectively, for fixed  $n_{\text{relax}}$ .

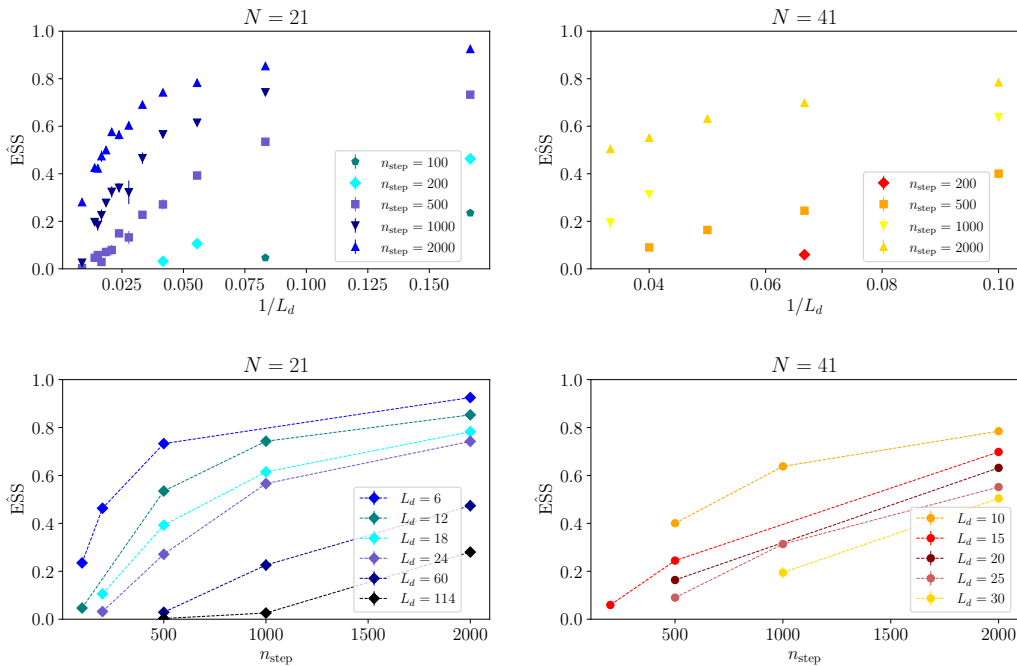


**Figure 4:** Behavior of the  $\hat{\text{E}}\text{SS}$  as a function of  $n_{\text{step}}$  (lower panels) and of the inverse of the defect size  $L_d$  (upper panels), for  $N = 21$  (left panels) and  $N = 41$  (right panels).

For sufficiently small defects,  $L_d < 20$ , the value of  $\hat{\text{E}}\text{SS}$  is seen to become greater than 0.5 already for  $n_{\text{step}} \simeq 500$ . For larger defects,  $L_d > 20$ , a value of  $n_{\text{step}}$  of order 1000–2000 is required for  $\hat{\text{E}}\text{SS}$  to be greater than 0.5. While  $\hat{\text{E}}\text{SS} = 0.5$  can be considered as a lower safety threshold, we will see below that the Monte Carlo ensembles that were employed were large enough to allow an acceptable computation of the topological susceptibility with even smaller values.

A careful inspection of the available data suggest that, in fact, both  $\hat{\text{E}}\text{SS}$  and  $\tilde{D}_{\text{KL}}$  are, to a good approximation, only functions of the ratio  $n_{\text{step}}/L_d$ . That this is a sensible idea can be immediately appreciated from Fig. 5, where  $\hat{\text{E}}\text{SS}$  and  $\tilde{D}_{\text{KL}}$  are shown to collapse on two different single  $n_{\text{step}}/L_d$  dependent curves at two different values of  $N$ . A semi-quantitative justification can instead be obtained from the definition of work in Eq. (2.10). Indeed, the calculation of  $W$  involves the sum of the variations of the action induced by the change  $c(n) \rightarrow c(n+1)$ . Focusing for simplicity on only the nearest-neighbors interaction terms, we can write:

$$S_L^{(n+1)}[\phi_n] - S_L^{(n)}[\phi_n] \propto \sum_{\substack{x_1=0 \\ x_0=L-1 \\ \mu=0}}^{L_d-1} \Delta c(n) \Re [U_\mu(x) \bar{z}(x + \hat{\mu}) z(x)], \quad (3.1)$$

with

$$\Delta c(n) = c(n+1) - c(n) = \frac{1}{n_{\text{step}}}, \quad (3.2)$$

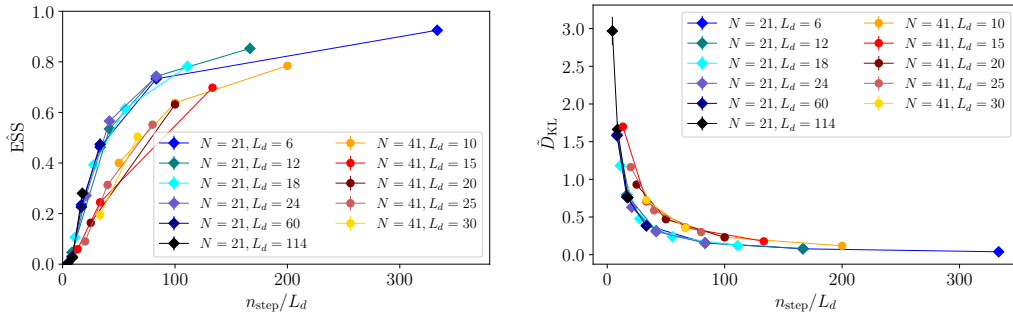


**Figure 5:** Behavior of the  $\hat{E}\hat{S}\hat{S}$  (left panel) and of  $\tilde{D}_{\text{KL}}$  (right panel) as a function of  $n_{\text{step}}/L_d$  at fixed value of  $n_{\text{relax}}$ .

and where we have assumed that the defect lies on the  $x_0 = L - 1$  boundary from  $x_1 = 0$  to  $x_1 = L_d - 1$ . Since a difference of actions is an extensive quantity and is, in the case at hand, localized on the defect, then the average of the quantity in Eq. (3.1) is of order  $L_d$ . Then, as a consequence of our choice of interpolating function,  $c(n) = n/n_{\text{step}}$ , it is clear that Eq. (3.1) is, on average, only a function of  $L_d \times \Delta c(n) = L_d/n_{\text{step}}$ . The same considerations can be made on the next-to-nearest-neighbors interaction term. Hence, the work  $W$  will on average only depend on  $n_{\text{step}}/L_d$  and it is natural to think that the same holds true for  $\hat{E}\hat{S}\hat{S}$  and  $\tilde{D}_{\text{KL}}$  as well.

Further insight on  $\hat{E}\hat{S}\hat{S}$  and  $\tilde{D}_{\text{KL}}$  can be obtained from Fig. 6 where the frequency histograms of the out-of-equilibrium evolution are displayed as functions of  $W$  and of the normalized<sup>3</sup> weight  $w = \exp\{-W + \Delta F\}$  that appears in Eq. (2.12).

Three different cases are represented, corresponding to evolutions that are far from ( $n_{\text{step}} = 50$ ), *moderately* far from ( $n_{\text{step}} = 500$ ) and close ( $n_{\text{step}} = 2000$ ) to equilibrium. The left-hand panel of the figure shows how the peak in the distribution of the evolutions in  $W$  approaches the value of  $\Delta F$ , represented as the vertical black line, as  $n_{\text{step}}$  grows, i.e. as the evolution approaches equilibrium. This corresponds, in the right-hand panel, to the distribution of evolutions in  $w$  becoming progressively more peaked around 1, where  $W = \Delta F$ , with the variance in  $w$  approaching zero.

The right-hand panel also enables us to better understand the reliability of the statistical reweighting procedure in Eq. (2.12). When the protocol is relatively far from equilibrium ( $n_{\text{step}} = 50$ ), the distribution in  $W$  has a larger support and, correspondingly, the support of the distribution in  $w$  then extends exponentially to smaller values. In this case, large statistics would be necessary to provide an unbiased sampling of  $w$ . To the opposite, a more peaked distribution in  $W$  is obtained as  $n_{\text{step}}$  is increased, corresponding to a smaller support in the distribution of  $w$ , and to an easier sampling. This is completely analogous to how the reliability of the re-weighting technique in classical statistical mechanics depends on the overlap between the supports of the source and target distributions.

In conclusion, both the  $\hat{E}\hat{S}\hat{S}$  and  $\tilde{D}_{\text{KL}}$  behave as expected on theoretical grounds and according to the general discussion in Sec. 2.2. This means, in practice, that we are

<sup>3</sup>The weight  $w$  is normalized so that  $\langle w \rangle_f = 1$  by virtue of Jarzynski's equality.

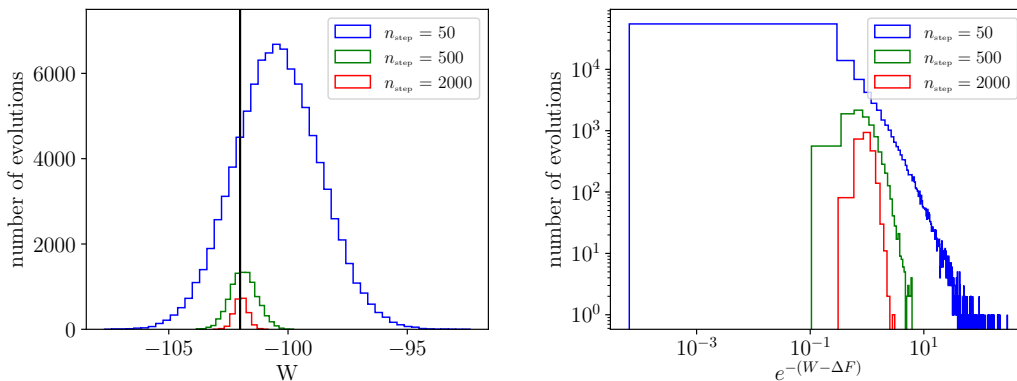


**Figure 6:** Distribution of the work  $W$  (left panel) and of  $\exp\{-(W - \Delta F)\}$  (right panel) for  $L_d = 6$  for various values of  $n_{\text{step}}$ . In the left panel the vertical bar represents the value of  $\Delta F$  for these particular evolutions.

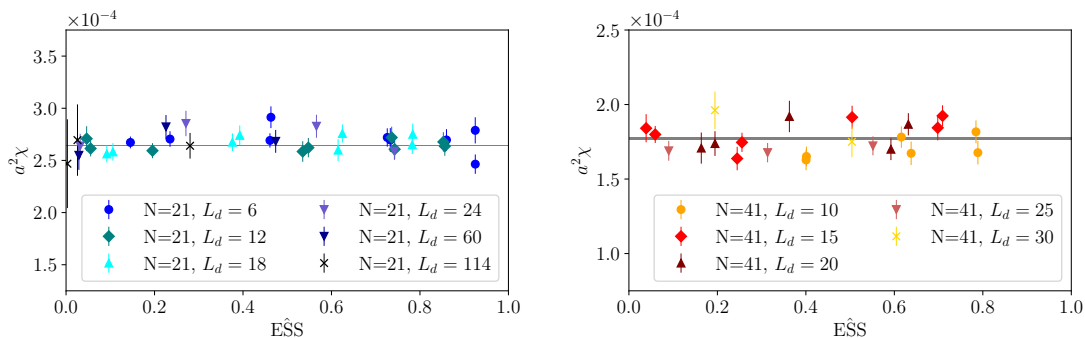


**Figure 7:** Results for the topological susceptibility in lattice units  $a^2\chi$  obtained with non-equilibrium evolutions as a function of the Effective Sample Size, for  $N = 21$  and  $\beta = 0.7$  (left panel) and for  $N = 41$  and  $\beta = 0.65$  (right panel). The results obtained with the PTBC algorithm in Ref. [32] is reported as a black horizontal line.

able to control the magnitude of systematic effects originated from the reweighting step in Eq. (2.12), and we can fully trust the expectation values obtained for the target distribution. In the next section, we will present a practical application of the strategy laid out above. Further details on the mutual relation between  $\hat{\text{ESS}}$  and  $\tilde{D}_{\text{KL}}$  can be found in Appendix B.

### 3.2 Extracting the topological susceptibility

A necessary condition for the viability of the non-equilibrium methods must of course rely on the comparison between its results and the results obtained with equilibrium methods. In Fig. 7 the values of the topological susceptibility  $\chi$  obtained using Eq. (2.12) and several combinations of  $L_d$ ,  $n_{\text{step}}$  and  $N$  are displayed, along with the values obtained in Ref. [32], using the PTBC algorithm.

The non-equilibrium results are found to be in excellent agreement with those from the PTBC algorithm for the whole range of values of  $\hat{\text{ESS}}$ . Notably, no bias seems to



arise even when  $\hat{\text{E}}\hat{\text{S}}\hat{\text{S}} \sim 0.1$  or smaller, while for nearly vanishing  $\hat{\text{E}}\hat{\text{S}}\hat{\text{S}}$ , an increase in the magnitude of the error seems to occur for  $L_d = 114$  at  $N = 21$ . This remarkable fact can be understood in terms of the computational effort spent to obtain each estimate of  $a^2\chi$ . The computational effort is of course proportional to  $n_{\text{stat}} = n_{\text{ev}} \times (n_{\text{step}} + n_{\text{relax}})$ , and this is roughly the same for each point on the plot in Fig 7. Hence, the data on the lower range of  $\hat{\text{E}}\hat{\text{S}}\hat{\text{S}}$ , for which  $n_{\text{step}}/L_d$  is small, is characterized by a correspondingly larger factor  $n_{\text{ev}}$ . This is in agreement with the previous observation that a comparatively larger statistics is needed to avoid bias in expectation values computed from Eq. 2.12, when using evolutions that are farther from equilibrium.

### 3.3 Integrated auto-correlation time of $\chi$

A quantitative study of the non-equilibrium method crucially revolves around the computation of the integrated auto-correlation time of the topological susceptibility. The auto-correlation function for  $\chi$ , from which the integrated auto-correlation time will be calculated, has been computed as follows,

$$\Gamma(t) \equiv \langle (Q_{i+t}^2/L^2 - a^2\chi)(Q_i^2/L^2 - a^2\chi) \rangle_{\text{NE}} \quad (3.3)$$

where  $Q_i^2$  denotes the cooled squared geometric lattice topological charge at the end of the  $i^{\text{th}}$  out-of-equilibrium evolution, i.e., when the system is subject to PBCs, and

$$a^2\chi = \frac{\langle Q^2 \rangle_{\text{NE}}}{L^2}. \quad (3.4)$$

is the topological susceptibility computed from out-of-equilibrium evolutions.

For convenience, it is useful to define *normalized* auto-correlation function  $\rho(t) \equiv \Gamma(t)/\Gamma(0)$ , which is displayed in Fig. 8 for various combinations of  $n_{\text{step}}$  and  $n_{\text{relax}}$  at fixed  $L_d$ . The integrated auto-correlation time is defined in terms of  $\rho(t)$  as follows,

$$\tau_{\text{int}} = \frac{1}{2} + \sum_{t=1}^{\widetilde{W}} \rho(t), \quad (3.5)$$

where  $\widetilde{W}$  is the window computed using the  $\Gamma$ -method, see Refs. [71, 72].

The value of  $\tau_{\text{int}}$  computed for several combinations of  $n_{\text{relax}}$ ,  $L_d$  are reported in Tab. 2, and displayed as a function of  $1/L_d$ , for  $n_{\text{step}} = 1000$ , in Fig. 9. As one could expect, smaller values of  $\tau_{\text{int}}$  are generally observed for larger values of  $n_{\text{relax}}$ ,  $L_d$  and  $n_{\text{step}}$ , the latter corresponding to evolutions closer to equilibrium.

In the following, we will focus on the data obtained for combinations of parameters  $L_d$ ,  $n_{\text{relax}}$ ,  $n_{\text{step}}$  for which  $\tau_{\text{int}}$  is of order 1, as such small values of  $\tau_{\text{int}}$  afford a reliable estimate of the error on  $a^2\chi$ . No investigation of the full dependence of  $\tau_{\text{int}}$  on  $n_{\text{step}}$  will be attempted, as Tab. 2 shows that its value does not seem to change appreciably, even when  $n_{\text{step}}$  is doubled. Instead, we will focus on the regime  $n_{\text{relax}} \geq 50$ ,  $n_{\text{step}} \geq 500$ ,  $L_d \geq 6$  for the  $N = 21$  ensemble and  $L_d \geq 10$  for the  $N = 41$  ensemble.

The values of  $\tau_{\text{int}}$  are provided in Tab. 3 for  $N = 21$  at different values of the coupling and of the lattice volume. Remarkably, no significant variation is observed in either  $\tau_{\text{int}}$  or

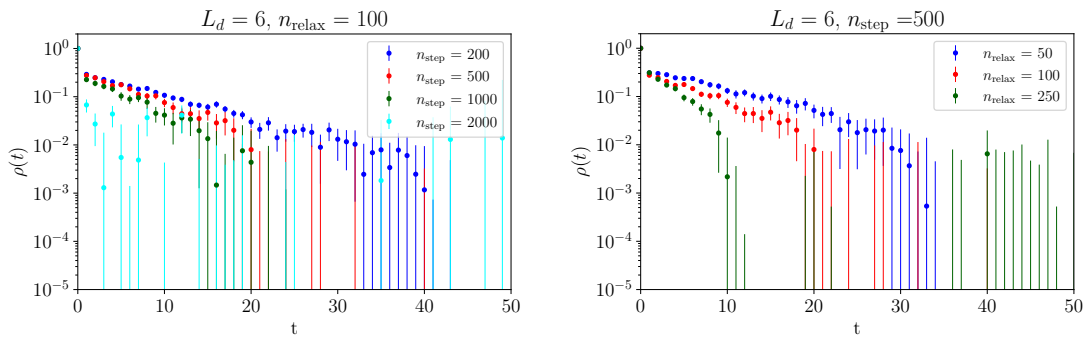


**Figure 8:** Behavior of the normalized auto-correlation function  $\rho(t)$  for  $L_d = 6$ , for several values of  $n_{\text{step}}$  at fixed  $n_{\text{relax}} = 100$  (left panel) and for several values of  $n_{\text{relax}}$  at fixed  $n_{\text{step}} = 500$  (right panel).

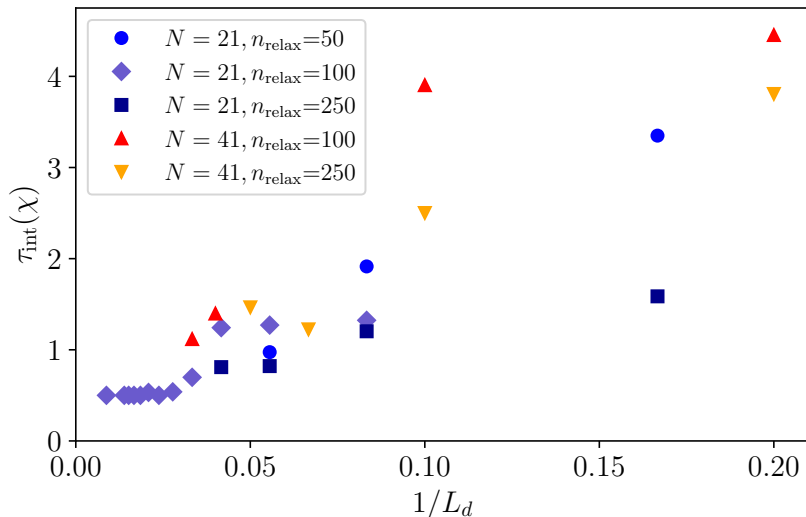


**Figure 9:** Behavior of the integrated auto-correlation time  $\tau_{\text{int}}(\chi)$  as a function of  $1/L_d$  for  $n_{\text{step}} = 1000$  and several values of  $n_{\text{relax}}$ , for the  $N = 21$  and the  $N = 41$  ensembles.

E $\hat{\text{S}}$ S as the coupling or the lattice volumes are varied at fixed  $(L_d, n_{\text{step}}, n_{\text{relax}})$ . This is a further confirmation of the previous observation that E $\hat{\text{S}}$ S seems to only depend on  $L_d$  and  $n_{\text{step}}$ , and provides evidence of the robustness of the non-equilibrium method.

### 3.4 Efficiency of the method

In this section, we assess the efficiency of the non-equilibrium method, using the product between the variance  $\chi$  and the cost of each evolution,  $\text{Var}(\chi)_{\text{NE}} \times (n_{\text{step}} + n_{\text{relax}})$ , as a figure of merit. Note that this is the quantity to minimize in order to reach the maximum efficiency in evaluating  $\chi$ , and this is the quantity on which a comparison with the PTBC approach will be based.

The quantity  $\text{Var}(\chi)_{\text{NE}}$  is computed directly from the sample of values of  $\chi$  obtained

$L_d$	$n_{\text{step}}$	$n_{\text{relax}}$	$\tau_{\text{int}}$	$L_d$	$n_{\text{step}}$	$n_{\text{relax}}$	$\tau_{\text{int}}$
6	500	50	5.3(8)	10	500	100	3.4(4)
6	500	100	3.6(5)	10	500	250	2.1(2)
6	500	250	1.9(2)	10	1000	100	3.9(6)
6	1000	100	2.8(4)	10	1000	250	2.5(3)
12	1000	50	1.9(3)	15	500	100	1.8(2)
12	1000	100	1.3(1)	15	500	250	1.1(1)
12	1000	250	1.2(1)	15	1000	100	2.0(2)
24	1000	50	0.64(4)	15	1000	250	1.2(2)
24	1000	100	1.2(1)	20	1000	100	1.7(3)
24	1000	250	0.81(4)	30	1000	100	1.1(1)
36	1000	100	0.54(3)				

**Table 2:** Values of the integrated auto-correlation time extracted with the  $\Gamma$ -method for several combinations of  $L_d$ ,  $n_{\text{step}}$  and  $n_{\text{relax}}$ , for the  $N = 21$  ensembles (left table) and the  $N = 41$  ensembles (right table). According to the results of Ref. [15], where the joint dependence of the auto-correlation time of  $\chi$  on  $\beta$  and  $N$  was studied using the same lattice volumes, lattice discretization and over-relaxation/heat-bath updating algorithms employed in the present investigation, for  $N = 21$  and  $\beta = 0.7$  we expect  $\tau_{\text{int}}^{(\text{PBCs})} \sim 10^4 - 10^5$  standard updating steps using PBCs, while for  $N = 41$  and  $\beta = 0.65$  an even larger auto-correlation time. For a fair comparison, the quantity  $\tau_{\text{int}}^{(\text{PBCs})}$  has to be compared with  $\tau_{\text{int}} \times (n_{\text{step}} + n_{\text{relax}})$ .

$\beta$	$L$	$L_d$	$n_{\text{step}}$	$n_{\text{relax}}$	$\tau_{\text{int}}$	$\hat{\text{E}}\hat{\text{S}}\hat{\text{S}}$
0.65	114	24	1000	50	0.52(4)	0.72(1)
0.7	114	24	1000	50	0.64(4)	0.731(6)
0.7	161	24	1000	50	0.68(5)	0.73(1)
0.75	114	24	1000	50	0.56(3)	0.71(1)

**Table 3:** Comparison of  $\tau_{\text{int}}$  and  $\hat{\text{E}}\hat{\text{S}}\hat{\text{S}}$  for different values of the coupling  $\beta$  and the size of the lattice  $L$

after reweighting according to Eq. (2.12). Some insight into this figure of merit can be gained from using Eq. (2.19), and taking into account the effects of auto-correlation. It then follows that

$$\text{Var}(\chi)_{\text{NE}} \times (n_{\text{step}} + n_{\text{relax}}) \simeq \text{Var}(\chi)_p \frac{2\tau_{\text{int}}}{\hat{\text{E}}\hat{\text{S}}\hat{\text{S}}} \times (n_{\text{step}} + n_{\text{relax}}). \quad (3.6)$$

where  $\text{Var}(\chi)_p$  would be the variance of the topological susceptibility when sampled *directly* from the target distribution  $p$  (i.e., with PBCs). Note that in principle, this is a quantity which is only dependent on the latter distribution, and independent from the parameters of the non-equilibrium algorithm. Indeed, the effect of the auto-correlations and of using Eq. (2.12) to estimate observables are accounted for, respectively, by the presence of  $\tau_{\text{int}}$  and  $\hat{\text{E}}\hat{\text{S}}\hat{\text{S}}$ .

This figure of merit is displayed in Fig. 10 as a function of  $n_{\text{step}}$ , for several combinations of  $L_d$  and  $n_{\text{relax}}$ . The values obtained for the non-equilibrium estimations do not seem to

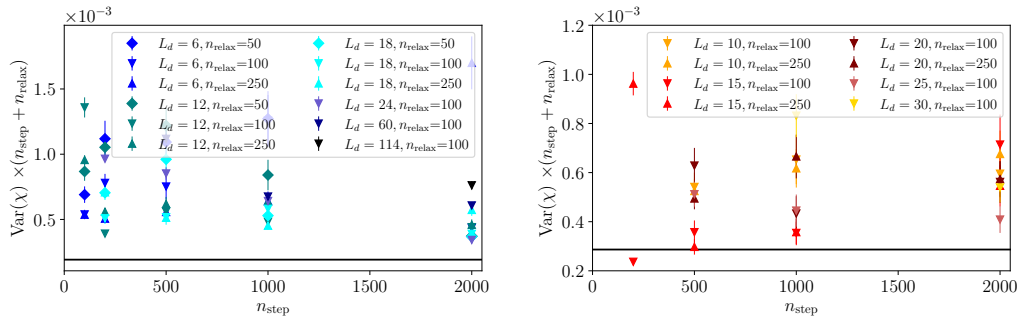


**Figure 10:** Behavior of the variance of the topological susceptibility, multiplied by the cost per evolution (in units of the Monte Carlo update), as a function of  $n_{\text{step}}$  for several values of  $n_{\text{relax}}$  and  $L_d$ , for  $N = 21$ ,  $\beta = 0.7$  (left panel) and  $N = 41$ ,  $\beta = 0.65$  (right panel). The black line is the same quantity for the PTBC algorithm, from Refs. [32, 33].

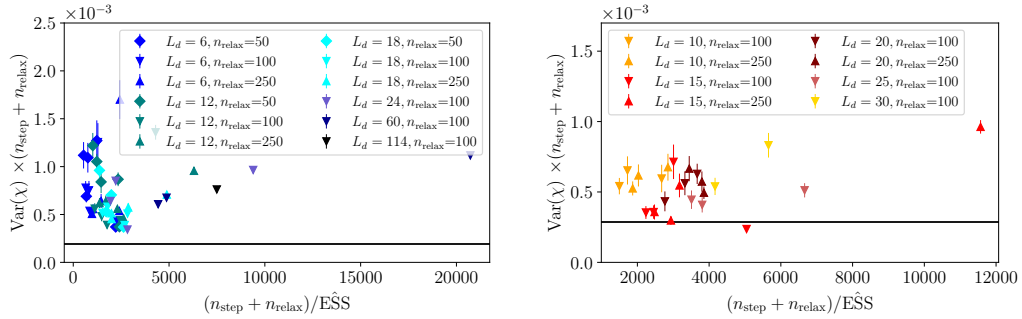


**Figure 11:** Variance of the topological susceptibility, multiplied by the cost per evolution (in units of Monte Carlo updates), as a function of  $(n_{\text{step}} + n_{\text{relax}})/\hat{\text{ESS}}$  for several values of  $n_{\text{relax}}$  and  $L_d$ , for  $N = 21$ ,  $\beta = 0.7$  (left panel) and  $N = 41$ ,  $\beta = 0.65$  (right panel). The black line is the same quantity for the PTBC algorithm, from Refs. [32, 33].

have any definite behaviour as  $n_{\text{step}}$  is increased. However, they cluster around a value that is larger, but within  $1.5 \times 10^{-3}$ , of those obtained with the PTBC approach, see Refs. [32, 33].

Further insight into the efficiency of the non-equilibrium method can be gained by separating the effects of the reweighting step in Eq. (2.12) from the rest of the non-equilibrium procedure. This can be achieved simply by displaying the figure of merit in Eq. (3.6) as a function of  $(n_{\text{step}} + n_{\text{relax}})/\hat{\text{ESS}}$ . This is done in Fig. 11, from which it can be inferred that  $\text{Var}(\chi)_{\text{NE}}$  is not a function of  $\hat{\text{ESS}}$  alone. The reason is twofold. First, the quantity we are using,  $\hat{\text{ESS}}$  is but an estimator of the “true” effective sample size. We refer to Appendix A for further discussion. Second, a quantitative characterization of the behaviour of  $\tau_{\text{int}}$  as a function of  $n_{\text{relax}}$ ,  $L_d$  and  $n_{\text{step}}$  is not attempted in this work. Although this would be needed to unravel the full dependence of the figure of merit on the specific parameters used in the non-equilibrium evolution, we believe that the above analysis is a solid step in that direction, as it provides the region in which the optimal values of  $L_d$ ,  $n_{\text{relax}}$  and  $n_{\text{step}}$  may be found.

## 4 Conclusions

In this work, we have presented a first exploration of a non-equilibrium Monte Carlo setup designed to mitigate the problem known as topological freezing. We have carried out our analysis using the  $2d$   $CP^{N-1}$  model as test bed, owing to their combination of numerical simplicity and physical non-triviality. The new approach outlined in this manuscript has some features in common with the PTBC algorithm originally proposed by M. Hasenbusch. It consists in starting from a thermalized ensemble generated with OBCs, and gradually switching to PBCs along a non-equilibrium Monte Carlo evolution. At the end of the latter, expectation values with PBCs can be computed through a reweighting-like formula which is tightly related to Jarzynski's equality.

This method is able to reproduce the expected value of the topological susceptibility of the  $CP^{N-1}$  models. Moreover, it is possible to gauge the reliability of the said reweighting-like formula using two different figures of merit: the Effective Sample Size and the Kullback–Leibler divergence, which provide consistent results. The efficiency of the method, quantified in terms of the product of the variance of the final result with the computational effort of one measurement is also shown to be comparable to the one found in the PTBC approach.

Put in perspective, the above study provides a broad framework for the application of non-equilibrium methods to address the issue of critical slowing down in lattice simulations. It can be thought as a different kind of Monte Carlo simulation, and could be implemented, for instance, by varying the value of  $\beta$  rather than of some parameter controlling the type of boundary conditions. In principle, one could start by an equilibrium sampling of the configuration space of the system for values of the inverse coupling characterized by small auto-correlations. Then, the coupling could be gradually increased through non-equilibrium evolutions, to values at which the system would be strongly auto-correlated at equilibrium. The meaning of  $n_{\text{step}}$  and  $n_{\text{relax}}$  would then be the same as above, while  $L_d$  would be replaced by a new parameter  $\Delta\beta$  describing the non-equilibrium changes in  $\beta$ . We highlight that this approach has already been implemented in the  $4d$   $SU(3)$  pure-gauge theory in Ref. [40], although not with the aim of mitigating the effects of critical slowing down.

Given the recently-established connection with Jarzynski's equality and the theoretical framework of Stochastic Normalizing Flows (SNFs) in Ref. [44], our work sets the stage for an application of our proposal to SNFs, where a stochastic part (which is given by the out-of-equilibrium evolutions discussed in this study) is combined with the discrete layers (parametrized by neural networks) that compose Normalizing Flows. The training of such layers would of course need a possibly lengthy procedure, which is however performed only once. Such an approach has the potential to greatly improve the efficiency of the non-equilibrium evolutions as, in principle, a considerably lower amount of Monte Carlo steps would be needed to achieve the same efficiency when sampling the target distribution. Another natural future outlook of the present investigation is to implement the non-equilibrium setup in a more physical and realistic model, such as the  $4d$   $SU(3)$  pure-gauge theory. We plan to investigate both ideas in the near future.

## Acknowledgments

The work of C. B. is supported by the Spanish Research Agency (Agencia Estatal de Investigación) through the grant IFT Centro de Excelencia Severo Ochoa CEX2020-001007-S and, partially, by grant PID2021-127526NB-I00, both funded by MCIN/AEI/10.13039/501100011033. A. N. acknowledges support by the Simons Foundation grant 994300 (Simons Collaboration on Confinement and QCD Strings) and from the SFT Scientific Initiative of INFN. The work of D. V. is supported by STFC under Consolidated Grant No. ST/X000680/1. The numerical simulations were run on machines of the Consorzio Interuniversitario per il Calcolo Automatico dell’Italia Nord Orientale (CINECA).

## Appendix

### A Evaluating $\hat{\text{ESS}}$ as an estimator of the Effective Sample Size

From Eq. (3.6), the variance  $\text{Var}(\chi)_p$  obtained in a system with PBCs can be related to the variance of the same quantity, but computed with non-equilibrium methods, as follows,

$$\text{Var}(\chi)_p = \langle (a^2\chi)^2 \rangle - \langle a^2\chi \rangle^2 \simeq \text{Var}(\chi)_{\text{NE}} \frac{\hat{\text{ESS}}}{2\tau_{\text{int}}}. \quad (\text{A.1})$$

Now, as already stated in the main text, this quantity should be (approximately) independent of the method used to compute  $a^2\chi$  and of the magnitude of the involved auto-correlations. In particular, this is certainly valid if the “true” ESS is used in the right-hand side. We now wish to check that this remains true also when ESS is replaced by its estimator  $\hat{\text{ESS}}$ . If  $\hat{\text{ESS}}$  was a good estimator, then we would expect the left-hand side to be independent of any change in the parameters of the non-equilibrium evolutions. In Fig. 12,  $\text{Var}(\chi)_p$  is displayed as a function of  $\hat{\text{ESS}}$  for  $N = 21$  at  $\beta = 0.7$ , and  $N = 41$  at  $\beta = 0.65$ . The range of  $\hat{\text{ESS}}$  explored is evidence of the fact that the parameters that are being tuned do impact on the non-equilibrium evolutions. Yet, for each value of  $N$  separately, the values of  $\text{Var}(\chi)$  seem to cluster around a constant, with no discernible dependence on  $\hat{\text{ESS}}$ . We thus conclude that  $\hat{\text{ESS}}$  must be a good estimator of the true effective sample size, at least in the range of parameters that was explored.

### B Relation between the Effective Sample Size and the Kullback–Leibler divergence

In this study we considered two different figures of merit to quantify the distance from equilibrium of our out-of-equilibrium evolutions: the Kullback–Leibler divergence  $\tilde{D}_{\text{KL}}$  of Eq. (2.17) and the estimator of the Effective Sample Size  $\hat{\text{ESS}}$  of Eq. (2.20). Given that the latter depends on the features of the probability distribution of the weights  $e^{-W}$  appearing in Eq. (2.12), and the former on the probability distribution of the work  $W$  itself, it is clear that these two quantities are tightly related, although not in a straightforward way. Indeed, our data seems to point out that  $\tilde{D}_{\text{KL}}$  and  $\hat{\text{ESS}}$  are in a one-to-one correspondence, with little to no dependence on the details of the simulation (i.e., on  $L_d$  and  $n_{\text{step}}$ ). In

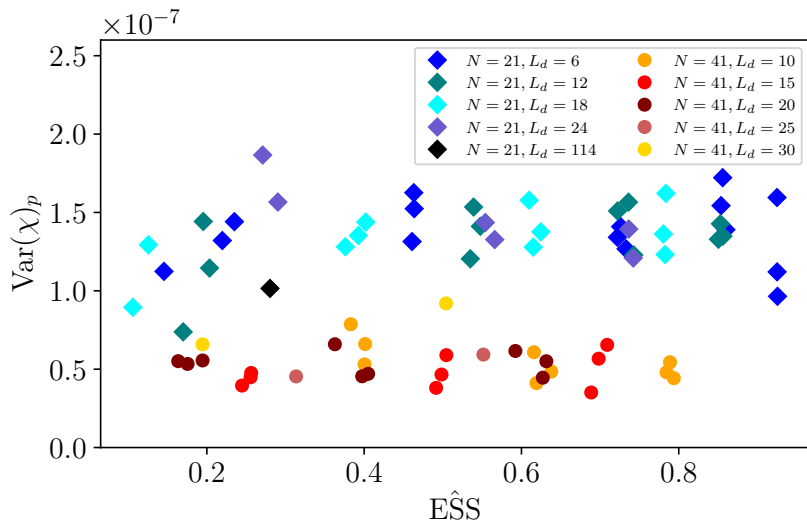


**Figure 12:** Variance of the topological susceptibility sampled on PBCs, as a function of  $E\hat{S}S$  for several values of  $n_{\text{step}}$ ,  $n_{\text{relax}}$  and  $L_d$ , both for the  $N = 21$  and  $N = 41$  ensembles.

the left-hand panel of Fig. 13,  $\tilde{D}_{\text{KL}}$  is displayed as a function of  $E\hat{S}S$ . To an impressive degree of precision, the data points seem to gather around the graph of an invertible function that relates  $E\hat{S}S$  to  $\tilde{D}_{\text{KL}}$ . This signals that these two quantities are in a one-to-one correspondence.

Another aspect of the same tight relationship can be appreciated by first highlighting a result from Ref. [25],

$$\tilde{D}_{\text{KL}} \simeq \frac{1}{2} \text{Var}(W), \quad (\text{B.1})$$

which was derived in the case of Normalizing Flows. The above is strikingly demonstrated in left-hand panel of Fig. 6, where  $\tilde{D}_{\text{KL}}$  is displayed as a function of  $\text{Var}(W)$ . The data seem to organize along a line with slope 1/2, with remarkable precision, as expected from Eq. B.1.

Since the estimator of the Effective Sample Size is directly related to the variance of the exponential average, see Eq. (2.21), it is natural to think that it can be linked to the variance of the work itself. In order to better understand this relationship, let us introduce the fluctuation of the work  $\delta W \equiv W - \langle W \rangle_{\text{f}}$ , where, by definition,  $\langle \delta W \rangle_{\text{f}} = 0$ . It is straightforward to rewrite the  $E\hat{S}S$  as follows,

$$\langle e^{-2W} \rangle_{\text{f}} = e^{-2\langle W \rangle_{\text{f}}} \langle e^{-2\delta W} \rangle_{\text{f}}, \quad \implies \quad \frac{1}{E\hat{S}S} = e^{-2\tilde{D}_{\text{KL}}} \langle e^{-2\delta W} \rangle_{\text{f}}. \quad (\text{B.2})$$

If our protocol is sufficiently close to equilibrium, we know from Eq. (B.1) that the work  $W$  does not fluctuate much among different non-equilibrium evolutions. Hence, if we assume that  $\text{Var}(W) \equiv \langle \delta W^2 \rangle_{\text{f}} \ll 1$ , then the typical value of  $\delta W$  along these evolutions is small. Thus, it is reasonable to perform the following expansion,

$$\langle e^{-2W} \rangle_{\text{f}} \simeq e^{-2\langle W \rangle_{\text{f}}} (1 + 2 \text{Var}(W)), \quad \text{Var}(W) \ll 1. \quad (\text{B.3})$$

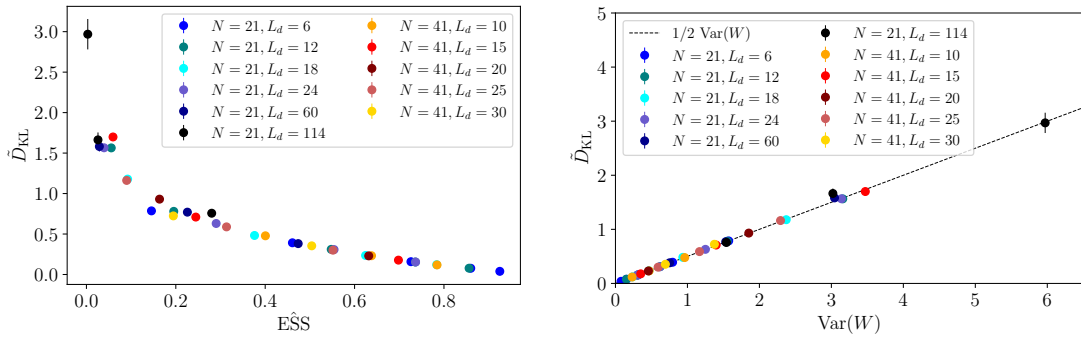


**Figure 13:** Behavior of  $\tilde{D}_{\text{KL}}$  as a function of  $\hat{\text{ESS}}$  (left panel) and as a function of the variance of the work  $\text{Var}(W)$  (right panel) for several values of the defect size  $L_d$ , both for the  $N = 21$  and  $N = 41$  ensembles.

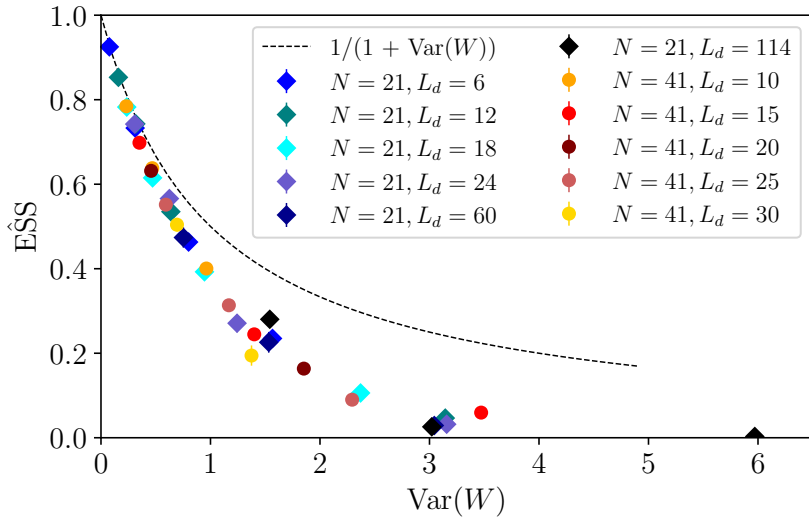


**Figure 14:** Behavior of the estimator  $\hat{\text{ESS}}$  as a function of the variance of the work  $\text{Var}(W)$ . The dashed line in the left panel represents our prediction from Eq. (B.4) in the close-to-equilibrium regime.

From Eq. (B.1) we now obtain a simple relation between  $\hat{\text{ESS}}$  and the variance of the work in the close-to-equilibrium limit,

$$\frac{1}{\hat{\text{ESS}}} \simeq 1 + \text{Var}(W), \quad \text{Var}(W) \ll 1. \quad (\text{B.4})$$

The validity of this approximate relation is confirmed by our data, see Fig. 14, and is further evidence, at least in the regime of close-to-equilibrium evolutions, the estimator  $\hat{\text{ESS}}$  is simply a function of  $\text{Var}(W)$ .



## References

- [1] B. Alles, G. Boyd, M. D’Elia, A. Di Giacomo and E. Vicari, *Hybrid Monte Carlo and topological modes of full QCD*, *Phys. Lett. B* **389** (1996) 107 [[hep-lat/9607049](#)].
- [2] P. de Forcrand, M. Garcia Perez, J. E. Hetrick and I.-O. Stamatescu, *Topology of full QCD*, *Nucl. Phys. Proc. Suppl.* **63** (1998) 549 [[hep-lat/9710001](#)].
- [3] B. Lucini and M. Teper, *SU(N) gauge theories in four-dimensions: Exploring the approach to  $N = \infty$* , *JHEP* **06** (2001) 050 [[hep-lat/0103027](#)].
- [4] D. B. Leinweber, A. G. Williams, J.-b. Zhang and F. X. Lee, *Topological charge barrier in the Markov chain of QCD*, *Phys. Lett. B* **585** (2004) 187 [[hep-lat/0312035](#)].
- [5] B. Lucini, M. Teper and U. Wenger, *Topology of SU(N) gauge theories at  $T \simeq 0$  and  $T \simeq T_c$* , *Nucl. Phys. B* **715** (2005) 461 [[hep-lat/0401028](#)].
- [6] L. Del Debbio, G. M. Manca and E. Vicari, *Critical slowing down of topological modes*, *Phys. Lett. B* **594** (2004) 315 [[hep-lat/0403001](#)].
- [7] L. Del Debbio, G. M. Manca, H. Panagopoulos, A. Skouroupathis and E. Vicari,  *$\theta$ -dependence of the spectrum of SU(N) gauge theories*, *JHEP* **06** (2006) 005 [[hep-th/0603041](#)].
- [8] ALPHA collaboration, S. Schaefer, R. Sommer and F. Virotta, *Critical slowing down and error analysis in lattice QCD simulations*, *Nucl. Phys. B* **845** (2011) 93 [[1009.5228](#)].
- [9] M. Lüscher and S. Schaefer, *Lattice QCD without topology barriers*, *JHEP* **07** (2011) 036 [[1105.4749](#)].
- [10] A. Laio, G. Martinelli and F. Sanfilippo, *Metadynamics surfing on topology barriers: the  $CP^{N-1}$  case*, *JHEP* **07** (2016) 089 [[1508.07270](#)].
- [11] J. Flynn, A. Jüttner, A. Lawson and F. Sanfilippo, *Precision study of critical slowing down in lattice simulations of the  $CP^{N-1}$  model*, [1504.06292](#).
- [12] C. Bonati, M. D’Elia, P. Rossi and E. Vicari,  *$\theta$  dependence of 4D SU(N) gauge theories in the large-N limit*, *Phys. Rev. D* **94** (2016) 085017 [[1607.06360](#)].
- [13] M. Hasenbusch, *Fighting topological freezing in the two-dimensional  $CP^{N-1}$  model*, *Phys. Rev. D* **96** (2017) 054504 [[1706.04443](#)].
- [14] C. Bonati and M. D’Elia, *Topological critical slowing down: variations on a toy model*, *Phys. Rev. E* **98** (2018) 013308 [[1709.10034](#)].
- [15] C. Bonanno, C. Bonati and M. D’Elia, *Topological properties of  $CP^{N-1}$  models in the large-N limit*, *JHEP* **01** (2019) 003 [[1807.11357](#)].
- [16] C. Bonanno, C. Bonati and M. D’Elia, *Large-N SU(N) Yang-Mills theories with milder topological freezing*, *JHEP* **03** (2021) 111 [[2012.14000](#)].
- [17] A. Athenodorou and M. Teper, *SU(N) gauge theories in 3+1 dimensions: glueball spectrum, string tensions and topology*, *JHEP* **12** (2021) 082 [[2106.00364](#)].
- [18] Bennett, D. K. Hong, J.-W. Lee, C. J. D. Lin, B. Lucini, M. Piai et al., *Sp(2N) Yang-Mills theories on the lattice: Scale setting and topology*, *Phys. Rev. D* **106** (2022) 094503 [[2205.09364](#)].
- [19] M. Lüscher and S. Schaefer, *Lattice QCD with open boundary conditions and twisted-mass reweighting*, *Comput. Phys. Commun.* **184** (2013) 519 [[1206.2809](#)].

- [20] T. Eichhorn, G. Fuwa, C. Hoelbling and L. Varnhorst, *Parallel Tempered Metadynamics: Overcoming potential barriers without surfing or tunneling*, [2307.04742](#).
- [21] G. Cossu, D. Lancastera, B. Lucini, R. Pellegrini and A. Rago, *Ergodic sampling of the topological charge using the density of states*, *Eur. Phys. J. C* **81** (2021) 375 [[2102.03630](#)].
- [22] S. Borsanyi and D. Sexty, *Topological susceptibility of pure gauge theory using Density of States*, *Phys. Lett. B* **815** (2021) 136148 [[2101.03383](#)].
- [23] M. Lüscher, *Stochastic locality and master-field simulations of very large lattices*, *EPJ Web Conf.* **175** (2018) 01002 [[1707.09758](#)].
- [24] G. Kanwar, M. S. Albergo, D. Boyda, K. Cranmer, D. C. Hackett, S. Racanière et al., *Equivariant flow-based sampling for lattice gauge theory*, *Phys. Rev. Lett.* **125** (2020) 121601 [[2003.06413](#)].
- [25] K. A. Nicoli, C. J. Anders, L. Funcke, T. Hartung, K. Jansen, P. Kessel et al., *Estimation of Thermodynamic Observables in Lattice Field Theories with Deep Generative Models*, *Phys. Rev. Lett.* **126** (2021) 032001 [[2007.07115](#)].
- [26] G. Papamakarios, E. T. Nalisnick, D. J. Rezende, S. Mohamed and B. Lakshminarayanan, *Normalizing flows for probabilistic modeling and inference*, *J. Mach. Learn. Res.* **22** (2021) 1.
- [27] R. Abbott et al., *Normalizing flows for lattice gauge theory in arbitrary space-time dimension*, [2305.02402](#).
- [28] W. Bietenholz, P. de Forcrand and U. Gerber, *Topological Susceptibility from Slabs*, *JHEP* **12** (2015) 070 [[1509.06433](#)].
- [29] L. Funcke, K. Jansen and S. Kühn, *Topological vacuum structure of the Schwinger model with matrix product states*, *Phys. Rev. D* **101** (2020) 054507 [[1908.00551](#)].
- [30] D. Albantea, P. Hernández, A. Ramos and F. Romero-López, *Topological sampling through windings*, *Eur. Phys. J. C* **81** (2021) 873 [[2106.14234](#)].
- [31] P. A. Boyle, *Advances in algorithms for solvers and gauge generation*, [2401.16620](#).
- [32] M. Berni, C. Bonanno and M. D’Elia, *Large- $N$  expansion and  $\theta$ -dependence of 2d  $CP^{N-1}$  models beyond the leading order*, *Phys. Rev. D* **100** (2019) 114509 [[1911.03384](#)].
- [33] C. Bonanno, M. D’Elia, B. Lucini and D. VDACCHINO, *Towards glueball masses of large- $N$   $SU(N)$  pure-gauge theories without topological freezing*, *Phys. Lett. B* **833** (2022) 137281 [[2205.06190](#)].
- [34] C. Bonanno, *Lattice determination of the topological susceptibility slope  $\chi'$  of 2d  $CP^{N-1}$  models at large  $N$* , *Phys. Rev. D* **107** (2023) 014514 [[2212.02330](#)].
- [35] J. L. Dasilva Golán, C. Bonanno, M. D’Elia, M. García Pérez and A. Giorgieri, *The twisted gradient flow strong coupling with parallel tempering on boundary conditions*, *PoS LATTICE2023* (2024) 354 [[2312.09212](#)].
- [36] C. Bonanno, M. D’Elia and L. Verzichelli, *The  $\theta$ -dependence of the  $SU(N)$  critical temperature at large  $N$* , [2312.12202](#).
- [37] C. Bonanno, C. Bonati, M. Papace and D. VDACCHINO, *The  $\theta$ -dependence of the Yang-Mills spectrum from analytic continuation*, [2402.03096](#).
- [38] C. Jarzynski, *Nonequilibrium Equality for Free Energy Differences*, *Phys. Rev. Lett.* **78** (1997) 2690 [[cond-mat/9610209](#)].

- [39] M. Caselle, G. Costagliola, A. Nada, M. Panero and A. Toniato, *Jarzynski's theorem for lattice gauge theory*, *Phys. Rev. D* **94** (2016) 034503 [[1604.05544](#)].
- [40] M. Caselle, A. Nada and M. Panero, *QCD thermodynamics from lattice calculations with nonequilibrium methods: The SU(3) equation of state*, *Phys. Rev. D* **98** (2018) 054513 [[1801.03110](#)].
- [41] O. Francesconi, M. Panero and D. Preti, *Strong coupling from non-equilibrium Monte Carlo simulations*, *JHEP* **07** (2020) 233 [[2003.13734](#)].
- [42] A. Bulgarelli and M. Panero, *Entanglement entropy from non-equilibrium Monte Carlo simulations*, *JHEP* **06** (2023) 030 [[2304.03311](#)].
- [43] H. Wu, J. Köhler and F. Noé, *Stochastic normalizing flows*, *Advances in Neural Information Processing Systems* **33** (2020) 5933.
- [44] M. Caselle, E. Cellini, A. Nada and M. Panero, *Stochastic normalizing flows as non-equilibrium transformations*, *JHEP* **07** (2022) 015 [[2201.08862](#)].
- [45] A. D'Adda, M. Lüscher and P. Di Vecchia, *A 1/N Expandable Series of Nonlinear Sigma Models with Instantons*, *Nucl. Phys. B* **146** (1978) 63.
- [46] M. Lüscher, *The secret long range force in quantum field theories with instantons*, *Physics Letters B* **78** (1978) 465.
- [47] E. Vicari and H. Panagopoulos,  *$\theta$  dependence of SU(N) gauge theories in the presence of a topological term*, *Phys. Rept.* **470** (2009) 93 [[0803.1593](#)].
- [48] M. Shifman, *Advanced topics in quantum field theory.: A lecture course*. Cambridge Univ. Press, Cambridge, UK, 2, 2012.
- [49] M. Campostrini, A. Di Giacomo and H. Panagopoulos, *The Topological Susceptibility on the Lattice*, *Phys. Lett. B* **212** (1988) 206.
- [50] M. Campostrini, P. Rossi and E. Vicari, *Monte Carlo simulation of CP<sup>N-1</sup> models*, *Phys. Rev. D* **46** (1992) 2647.
- [51] M. Campostrini, P. Rossi and E. Vicari, *Topological susceptibility and string tension in the lattice CP<sup>N-1</sup> models*, *Phys. Rev. D* **46** (1992) 4643 [[hep-lat/9207032](#)].
- [52] B. Alles, M. D'Elia, A. Di Giacomo and R. Kirchner, *A Critical comparison of different definitions of topological charge on the lattice*, *Phys. Rev. D* **58** (1998) 114506 [[hep-lat/9711026](#)].
- [53] W. Bietenholz, U. Gerber, M. Pepe and U.-J. Wiese, *Topological Lattice Actions*, *JHEP* **12** (2010) 020 [[1009.2146](#)].
- [54] M. Berni, C. Bonanno and M. D'Elia,  *$\theta$ -dependence in the small-N limit of 2d CP<sup>N-1</sup> models*, *Phys. Rev. D* **102** (2020) 114519 [[2009.14056](#)].
- [55] C. Bonanno, M. D'Elia and F. Margari, *Topological susceptibility of the 2D CP<sup>1</sup> or O(3) nonlinear  $\sigma$  model: Is it divergent or not?*, *Phys. Rev. D* **107** (2023) 014515 [[2208.00185](#)].
- [56] C. Bonanno, A. Nada and D. Vadicchino, *Out-of-equilibrium simulations to fight topological freezing*, *PoS LATTICE2023* (2024) 005 [[2310.11979](#)].
- [57] B. Berg, *Dislocations and Topological Background in the Lattice O(3)  $\sigma$  Model*, *Phys. Lett. B* **104** (1981) 475.

- [58] Y. Iwasaki and T. Yoshie, *Instantons and Topological Charge in Lattice Gauge Theory*, *Phys. Lett. B* **131** (1983) 159.
- [59] S. Itoh, Y. Iwasaki and T. Yoshie, *Stability of Instantons on the Lattice and the Renormalized Trajectory*, *Phys. Lett. B* **147** (1984) 141.
- [60] M. Teper, *Instantons in the Quantized  $SU(2)$  Vacuum: A Lattice Monte Carlo Investigation*, *Phys. Lett. B* **162** (1985) 357.
- [61] E.-M. Ilgenfritz, M. Laursen, G. Schierholz, M. Müller-Preussker and H. Schiller, *First Evidence for the Existence of Instantons in the Quantized  $SU(2)$  Lattice Vacuum*, *Nucl. Phys. B* **268** (1986) 693.
- [62] M. Campostrini, A. Di Giacomo, H. Panagopoulos and E. Vicari, *Topological Charge, Renormalization and Cooling on the Lattice*, *Nucl. Phys. B* **329** (1990) 683.
- [63] B. Alles, L. Cosmai, M. D’Elia and A. Papa, *Topology in 2D  $CP^{N-1}$  models on the lattice: A Critical comparison of different cooling techniques*, *Phys. Rev. D* **62** (2000) 094507 [[hep-lat/0001027](#)].
- [64] APE collaboration, M. Albanese et al., *Glueball Masses and String Tension in Lattice QCD*, *Phys. Lett. B* **192** (1987) 163.
- [65] C. Morningstar and M. J. Peardon, *Analytic smearing of  $SU(3)$  link variables in lattice QCD*, *Phys. Rev. D* **69** (2004) 054501 [[hep-lat/0311018](#)].
- [66] M. Lüscher, *Trivializing maps, the Wilson flow and the HMC algorithm*, *Commun. Math. Phys.* **293** (2010) 899 [[0907.5491](#)].
- [67] M. Lüscher, *Properties and uses of the Wilson flow in lattice QCD*, *JHEP* **08** (2010) 071 [[1006.4518](#)].
- [68] C. Bonati and M. D’Elia, *Comparison of the gradient flow with cooling in  $SU(3)$  pure gauge theory*, *Phys. Rev. D* **D89** (2014) 105005 [[1401.2441](#)].
- [69] C. Alexandrou, A. Athenodorou and K. Jansen, *Topological charge using cooling and the gradient flow*, *Phys. Rev. D* **92** (2015) 125014 [[1509.04259](#)].
- [70] V. Elvira, L. Martino and C. P. Robert, *Rethinking the effective sample size*, *International Statistical Review* **90** (2022) 525.
- [71] ALPHA collaboration, U. Wolff, *Monte Carlo errors with less errors*, *Comput. Phys. Commun.* **156** (2004) 143 [[hep-lat/0306017](#)].
- [72] F. Joswig, S. Kuberski, J. T. Kuhlmann and J. Neuendorf, *pyerrors: A python framework for error analysis of Monte Carlo data*, *Comput. Phys. Commun.* **288** (2023) 108750 [[2209.14371](#)].